The structural behaviour of masonry bridges designed as hydrostatic shells

Proceedings of the IASS 2024 Symposium
Redefining the Art of Structural Design
August 26-30, 2024, Zurich, Switzerland
Philippe Block, Giulia Boller, Catherine DeWolf,
Jacqueline Pauli, Walter Kaufmann (eds.)

The structural behaviour of masonry bridges designed as hydrostatic shells

Emil ADIELS[*a], Mats ANDER[a], Fredrik BOMAN[a], Jacob FORSBERG[a]
Michele GODIO[b], Emil SVEDJER[a], Erik WIGH[a], Chris J. K. WILLIAMS[a]

[a] Department of Architecture and Civil Engineering, Chalmers University of Technology
Gothenburg, Sweden
emil.adiels@chalmers.se
[b] RISE, Research Institutes of Sweden

Abstract

Masonry bridges are among the most sustainable structures ever to have been built. The long service time, the resilience to carry larger loads than originally intended, and significantly lower life cycle cost compared to other bridge types suggest that we should consider the design and construction of new masonry bridges, even if their initial cost is greater than that of steel or concrete bridges

The aim of this work is to understand the structural behaviour and study the collapse of a single-span masonry hydrostatic shell, that is a shell designed specifically to carry a hydrostatic load. Due to the complexity of the masonry shell interacting with fill, it is necessary to use a combination of computational methods and load tests on physical models in their structural assessment. We perform a load test to failure on a physical model spanning 770 mm made from 3D printed blocks and analyse the model using the Discrete Element Method (DEM) in Dassault Systèmes Abaqus.

The physical model behaved well and predicts that the bridge could be used at full scale. The preliminary results from a computational DEM model are found to be qualitatively good, but greatly overestimate the collapse load of the bridge.

Keywords: masonry bridges, masonry vaults, form finding, load test, discrete element method

1. Introduction

Masonry bridges play a vital role in our built environment and infrastructure. According to a 2004 survey by the International Union of Railways [1], the 200,000 masonry arch bridges and culverts of the participating organisations represented 60 % of their bridge stock. Most of the bridges, 70 %, were at that time between 100 and 150 years old.

Masonry bridges have a long service life, the resilience to carry larger loads than originally intended, and significantly lower life cycle costs than other bridge types [1]. McKibbins et al. [2, p. 25] wrote

> Masonry arch bridges can be viewed as among the most sustainable structures ever to have been built. Many have already been in service for hundreds of years without significant repair or strengthening works - exceeding the design life requirements of modern structures. By contrast, many of the steel and concrete bridges built in the last century have required considerable expenditure on maintenance and repair or even replacement within the first 30-40 years of service.

The successful long-term structural and environmental performance of masonry bridges means that we should consider the design and construction of new masonry bridges, even if their initial cost is greater than that of steel or concrete bridges. In the paper, 'The construction of new masonry bridges inspired by Paul Séjourné' [3] we presented the new design concept of hydrostatic shells and its associated theoretical framework.

The hydrostatic shell transforms the arch, the spandrel walls and the wing walls of a traditional masonry arch bridge into a shell or vault. The hydrostatic shape is due to that masonry bridges contain a considerable amount of fill material. The fill adds weight to the arch and spreads the load. The pressure from the fill has resulted in a geometry with less curvature at the top of the arch and more acute curvature near the supports, which can be observed in built examples such as the Maidenhead Railway Bridge (Figure 1) by Brunel or in bridges designed by Paul Séjourné.

Due to the complexity of the masonry shell interacting with the fill, it is necessary to use a combination of computational methods and load tests on physical models in their structural assessment. These can be used in conjunction with existing methods such as the line of thrust or MEXE [4]. The aim of this paper is to explain the structural behaviour, describe the form finding technique for a single-span hydrostatic shell and examine the collapse mechanism.

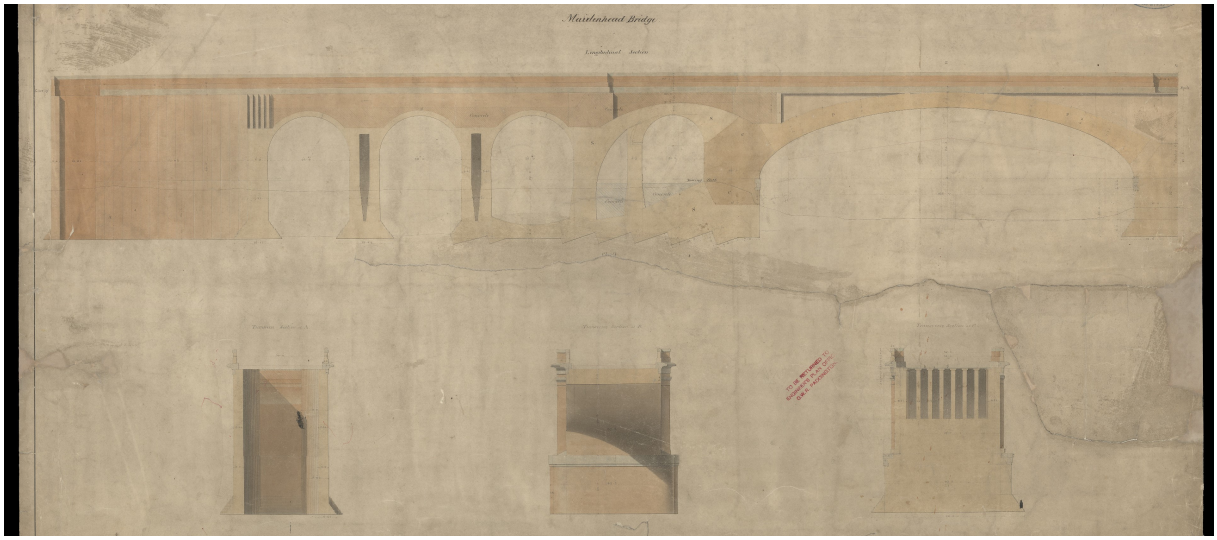

Figure 1: Elevation of Maidenhead Railway Bridge, image from Network Rail Corporate Archive.

2. Form finding of a single span hydrostatic shell

The concept of hydrostatic shells relies on the idea that the form is a membrane shell that is in equilibrium with the hydrostatic pressure. The equilibrium equation for a membrane shell can be written as

$$\frac{1}{\sqrt{a}}\left(\sigma^{\alpha\beta}\sqrt{a}\mathbf{a}_\beta\right)_{,\alpha} + p^\beta \mathbf{a}_\beta + p\mathbf{n} = 0. \tag{1}$$

Green & Zerna [5] use $n^{\alpha\beta}$ instead of $\sigma^{\alpha\beta}$ for the membrane stress tensor and $\mathbf{a}_3$ instead of $\mathbf{n}$ for the normal. For a hydrostatic shell, i.e only having a hydrostatic load excluding gravity one assumes $p = -\rho g z$, where ρg is the weight per unit volume and $p^\beta = 0$. Thus, we assume that the weight of the masonry is small compared to the total weight. We also assume that we have a mono-axial state of stress in the masonry so that one of the principal membrane stresses follows geodesics on the surface.

In form finding, the stresses and loading are known, and the geometry is unknown. For this problem, one could use techniques such as dynamic relaxation [6] or the force density method [7]. However, these methods tend to be unstable for this application since bulges tend to form between the geodesics. For

the special case of a single-span bridge it is much simpler to integrate (1), assuming a grid of geodesic coordinates and where the forces flow along the geodesics. Rewriting (1) to

$$T_b\mathbf{b} - T_a\mathbf{a} + \frac{\rho g z}{4}(\mathbf{a}+\mathbf{b}) \times \mathbf{c} = 0, \tag{2}$$

where $z \leq 0$. Vector $\mathbf{a}$ is $\mathbf{r}_{i,j} - \mathbf{r}_{i-1,j}$, $\mathbf{b}$ is $\mathbf{r}_{i+1,j} - \mathbf{r}_{i,j}$ and $\mathbf{c}$ is $\mathbf{r}_{i,j+1} - \mathbf{r}_{i,j-1}$ for a grid as in Figure 2. T_a and T_b are the force densities of $\mathbf{a}$ and $\mathbf{b}$. The unknown in this case is $\mathbf{b}$.

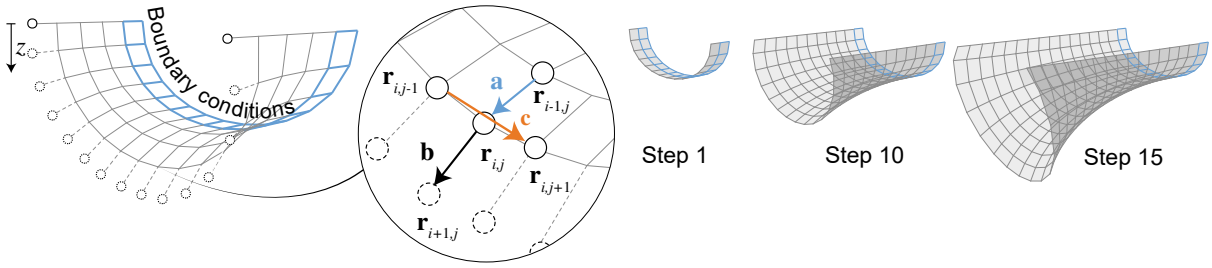

Figure 2: Form finding of hydrostatic shell with geodesic coordinates. Left, the right angles are given by the set boundary conditions (blue). Middle, the vectors $\mathbf{a}$ and $\mathbf{b}$ are the direction of the geodesics. The vector $\mathbf{c}$ is the direction of the orthogonal trajectories. Right, the form finding in progress at steps 1, 10 and 15.

Geodesic coordinates [8] mean that one of the coordinate curves follows geodesics, and the other coordinate curves intersect at a right angle and have a constant spacing. We only need to impose two of these conditions since the third results from the other two. In this case, it is assumed that the spacing is constant $|\mathbf{a}| = |\mathbf{b}| = L^2$. The condition of orthogonality comes from the set boundary conditions, blue in Figure 2, which is the transverse section profile to the span of the bridge at mid-span. Thus, the geometry is found by integrating along the geodesics (coming from the two other conditions), finding $\mathbf{b}$ to get the new position of $\mathbf{r}_{i+1,j}$.

The expression (2) can be simplified by assuming $T_a = T_b = T$

$$\mathbf{b} - \mathbf{a} + \frac{\rho g z}{4T}(\mathbf{a}+\mathbf{b}) \times \mathbf{c} = 0.$$

It is possible to attain the expression for $\mathbf{b}$ as a linear combination of $\mathbf{a}$, $\mathbf{c}$ and $\mathbf{a} \times \mathbf{c}$ as

$$\mathbf{b} = \frac{(1 - \mathbf{q}\cdot\mathbf{q})\,\mathbf{a} + 2\,(\mathbf{a}\cdot\mathbf{q})\,\mathbf{q} - 2\mathbf{a}\times\mathbf{q}}{1 + \mathbf{q}\cdot\mathbf{q}},$$

where $\mathbf{q} = (\rho g z/4T)\,\mathbf{c}$.

The form finding is illustrated in the right of Figure 2, showing the simulation at steps 1, 10 and 15. Depending on the choice of force density and the starting profile (blue) one get different results. After a certain amount of iterations, the surface will fold in on itself, similar to the case of a hydrostatic arch [9]. The form finding technique presented requires the designer to specify force density and the transversal section at mid-span of the bridge. The force density affects the span-to-rise ratio, where a lower force density will require a higher curvature of the geodesics. The specified profile shape and curvature affect the stiffness of the cross-section. More curvature should give more stiffness and thus attract forces, similar to the fold in a piece of paper. In Figure 3 are examples having different mid-span profiles. The effect of the curvature is most visible on the *superellipse* or *Lamé curve* to the right in Figure 3.

3. Prediction of the behaviour of masonry structures under load

There are several possible approaches for the prediction of structural behaviour: 'rules of thumb' or past experience, hand calculations, computational analysis, small-scale model tests, and full-scale tests.

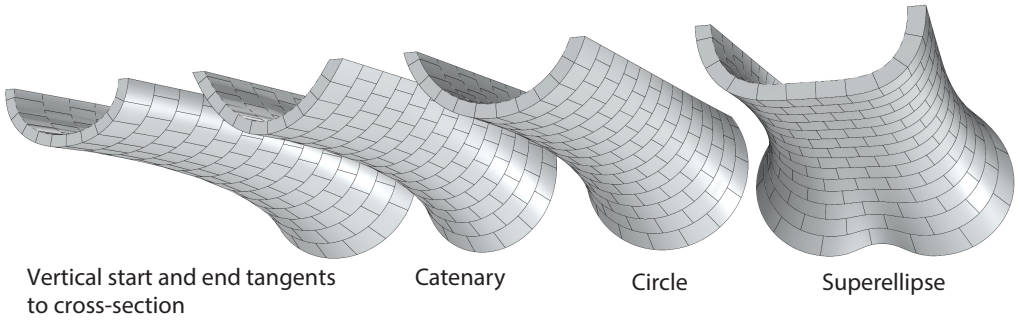

Figure 3: Perspective view of alternative bridges generated having different starting profiles at mid-span during form finding.

Hand calculations are usually based on plastic analysis (Figure 4 left). Heyman [10] states three key postulates that enable the upper and lower bound theorems of plasticity to be applied to masonry: masonry has no tensile strength, stresses are so low that masonry has effectively an unlimited compressive strength, and sliding failure does not occur. However, masonry bridges often contain a considerable amount of frictional fill material, and so, while one can use a lower bound approach, that is postulate a state of stress in equilibrium with the applied loads which does not violate the yield condition, but the answer is not necessarily a lower bound to the real collapse load. This is because if the fill yields according to the Mohr–Coulomb failure criterion this does not satisfy the normality postulate of plasticity.

Computational analysis may involve elastic analysis, but this is usually not appropriate since it does not take into account the opening of masonry joints. The *Discrete Element Method* (DEM) is commonly used for structural analysis of masonry structures in which the structure is modelled as a system of blocks, which can be rigid or deformable, or particles [11].

Small-scale model tests, or *masonry block models* [12], have been vital for master builders in the structural design and analysis of masonry vaults and arches. Most known is perhaps Danyzy's experiments [13] (Figure 4 right) with masonry arches to verify the masonry arch theory by Couplet [14]. The results scale directly between the model and the full scale, meaning scaling the span ten times the mass and other loads scale with a factor of a thousand. This is usually not the case for structures, but it is because structural analysis of masonry arches and vaults is usually not a question of strength but stability. This is because we assume that the stresses are relatively low in the architectural scale of, for instance, cathedrals, as Heyman [10] describes.

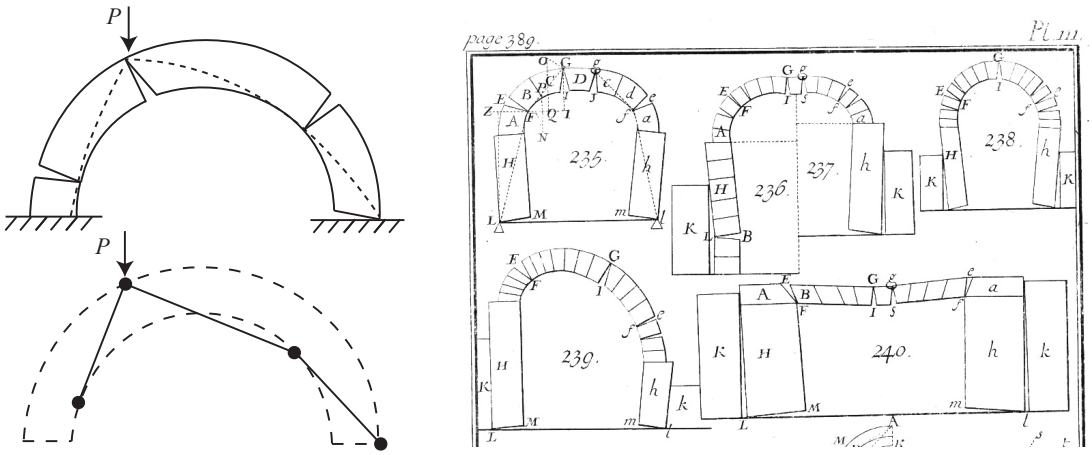

Figure 4: Left, the collapse mechanism for a masonry arch redrawn from Heyman [10]. Right, depictions of Danyzy's experiments of masonry arches from Frézier [13].

Proper scaling of the results involve *dimensional analysis* using Buckingham π theorem. First, we look at the scaling of the fill or the soil. From the Mohr-Coulomb criterion $\tau = c' + \sigma' \tan \phi'$, where τ is the shearing stress acting on the plane of failure and σ' is the effective normal stresses to the same plane. The effective stress is the total stress minus the pore water pressure. For a fill that is a granular soil that allows water and air to penetrate through the soil, the pore water pressure has less influence. The cohesion and friction angle are the material constants c' and ϕ', respectively.

The cohesion c' is affected by scaling. However, using dry sand as the fill could be seen as cohesionless soil [15], meaning $c' = 0$. In such cases, the soil is purely frictional and only the ratio between the shear and normal stresses matters. If the fill is purely frictional, one could imagine that it would be a conservative assumption and that real fill would be safer.

For the masonry, we can list relevant variables and their corresponding dimensions as in Table 1. Since we only have dimensions expressed in F and L, the number of independent non-dimensional groups are the number of variables subtracted by two, and we can also combine these to create other non-dimensional groups. In Table 2 examples of non-dimensional groups are presented.

Variables	**Dimensions**
Density times gravity, ρg	$\mathrm{F/L^3}$
Span, S	L
Collapse load, P	F
Compressive strength of masonry, σ	$\mathrm{F/L^2}$
Young's modulus of masonry, E	$\mathrm{F/L^2}$

Table 1: Possible variables for masonry bridge

Non-dimensional groups	**Variables**
Independent Group 1	$P/\rho g S^3$
Independent Group 2	$P/\sigma S^2$
Independent Group 3	σ/E
Alternative Group A	$\sigma/\rho g S$
Alternative Group B	$E/\rho g S$

Table 2: Non-dimensional groups

Group 1 in Table 2 expresses that if the span of our bridge increases by a factor of 30, the collapse load increases by 27,000.

$$\left(\frac{P}{\rho g S^3}\right)_{\text{full scale}} = \left(\frac{P}{\rho g S^3}\right)_{\text{model}} \tag{3}$$

However, if we believe the crushing of the stone is a probable risk, we can do the same for group 2, and the loads will scale by a factor of 900 instead. Group 3 is basically if we believe there is a failure in strain. Alternative group A would be stones failing under the weight of bridge and group B the bridge would not be stiff enough under its own weight.

4. Testing and analysis of model bridge

4.1. The bridge model

For the load test, the catenary profile was chosen in Figure 3. The fill depth to span ratio at the crown was 0.06, which is quite normal compared to other masonry arch bridges where it is common to lie between 0.04-0.06 (Figure 8 (d) in Brencich and Morbiducci [16]).

The span-to-rise ratio was chosen to be 0.11 (Figure 5), which can be considered a shallow bridge for masonry arch bridges. Shallow arch bridges are considered between 0.15 and 0.30, where the average value is 0.20 in historic and contemporary bridges [16]. As a reference, the Maidenhead Railway Bridge by Brunel has a span-to-rise ratio of 0.19, which was considered very shallow when built. However, since our bridge model is not an arch but a shell, it is difficult to compare directly.

The thickness of the bridge model was chosen to be 10 mm, giving it a ratio between the thickness in the crown and the span to be 0.013. This is considered low compared to other masonry arch bridges where most lie in the span 0.05-0.07 (Figure 8 (b) in Brencich and Morbiducci [16]).

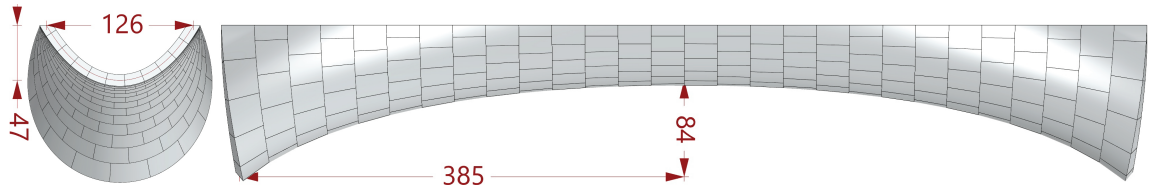

Figure 5: Section and elevation of the bridge that was tested had a catenary profile as input in form finding. Measurements are in mm.

The masonry blocks were 3D printed using the ProJet CJP 660. The material is similar to gypsum, and the printed parts can be fragile during handling; thus, the blocks were impregnated with 3D Systems ColorBond. The model was assembled (Figure 6) as dry masonry. The falsework was not removed until the fill had been applied, which in this model was finely-grained dry sand. The weight of the bridge was 2.49 kg masonry and 7.34 kg sand.

Figure 6: The construction process of a model bridge. Left, the 3D printed blocks are assembled without glue. Rounded extrusions are for easier assembly but do not contribute to any bending stiffness. The middle shows the bridge before filling it with sand as in the right image.

4.2. Load test setup

The model was built on a MDF board with a plywood board underneath to add strength. The timber abutments were screwed into these two boards, and thus a metal clamp was attached to increase the capacity to handle the lateral thrust during the test.

To apply the load, a rectangular timber frame was built that could fit around the model and carry a bucket placed underneath the model. The load was to be applied as a point load, and the chosen area was a square of 65x65 mm. On the underside of the frame, a scale was fitted with a metal hook for the bucket. It was decided to place the load at 1/4 the arch length, which is a critical placement for an arch.

The model had some initial geometric imperfections. In the top view (Figure 7 left), it is visible that one of the abutments is slightly rotated. Thus, on one side, it bulges outwards at mid-span, and on the other side, it curves slightly when it should be straight. From the elevation view (Figure 7 right), there is a slight downward bulge in the mid-span, where it should be nearly flat. Also, the blocks near the abutments on the left side have some imperfections.

Three cameras were used to capture the load test. One recorded the top view, the second the elevation view, and the third the scale display. Two measurement papers were placed at the midpoint and at the 1/4 point on the left side of the model. A string was attached between the abutments to capture their

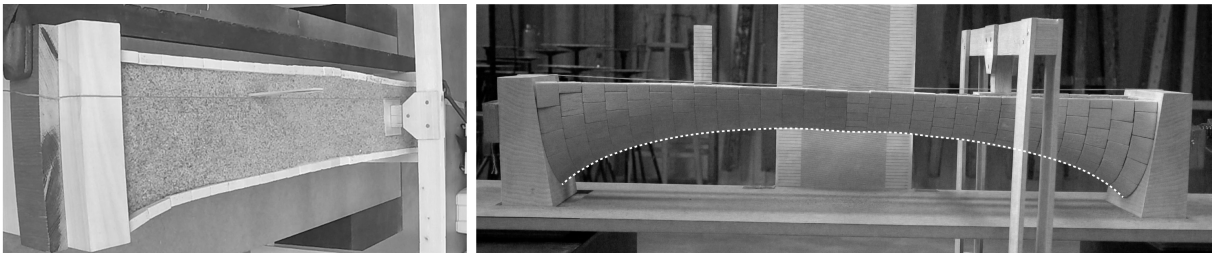

Figure 7: Left, view along the model seen from the left abutment. Right, the model in elevation. The white dashed line shows the contour which indicates the initial profile.

relative displacement.

4.3. Load test

The model was loaded twice before the collapse. The load was applied by a steady flow of sand. The bucket became full without collapse the first time of loading, which was approximately 19 kg. At this stage three phenomena were observed, exaggerated in blue in Figure 8 top. First, the abutments rotated slightly outwards on the left side and inwards on the right side. Second, there was a slight uplift on the left side of the bridge while the right moved slightly down. The bottom left picture shows the magnitude of the deformation, which is barely visible (Figure 8 bottom left). Third, there was local plastic deformation below the loading point, causing the profile to be nearly flat rather than curved (Figure 8 bottom right).

Before the second test, the model was unloaded. Since the collapse load was unknown, we started with a metal weight of 20 kg and, from there, a small increase of load using a flow of sand. There was not much displacement until around 27 kg when the displacement under the load increased, going from almost straight in profile to bulging outwards, and a crack began to become visible on the left side (both locations indicated in Figure 9 top). At a load of 28.5 kg, sand starts to come out of the crack under the load. At 28.7 kg, there is a constant flow of sand coming from the crack until 28.9 kg, where the crack opens completely (Figure 9 top) and the rig punches through (Figure 9 middle) and there is a sudden collapse (Figure 9 bottom). See the full video from the load test [17].

Thus, if we scale the model by a factor of 50 to match the span of the Maidenhead Railway bridge of 39 m using (3), the collapse load would be $28.9 \times 125{,}000 \times 10^{-3} = 3{,}600$ tonnes.

Discussion of failure modes

Taken as a whole, the bridge is a 3-dimensional thin shell but, in a 2-dimensional projection, acts as a thick arch and therefore the simple failure modes shown in Figure 4 are not kinematically possible. This explains why we have the localised bulging failure shown in Figure 9. This bulging failure is possibly influenced by the horizontal movement of the supports.

4.4. Computational analysis - Discrete element method

The bridge was modelled by the proprietary software Abaqus 2023, using Abaqus/Explicit, which is an explicit solver that is suitable to capture the non-linear behaviour as well as the opening of the joints of the masonry structure.

The geometry was based on the size of the bridge model. The voussoirs are defined as deformable bodies and given properties of Young's modulus of 70 GPa, Poisson's ratio of 0.3 and a density of 2750 kg/m^3.

The supports were modelled as a fixed surface on which the adjoining blocks are free to rotate and move.

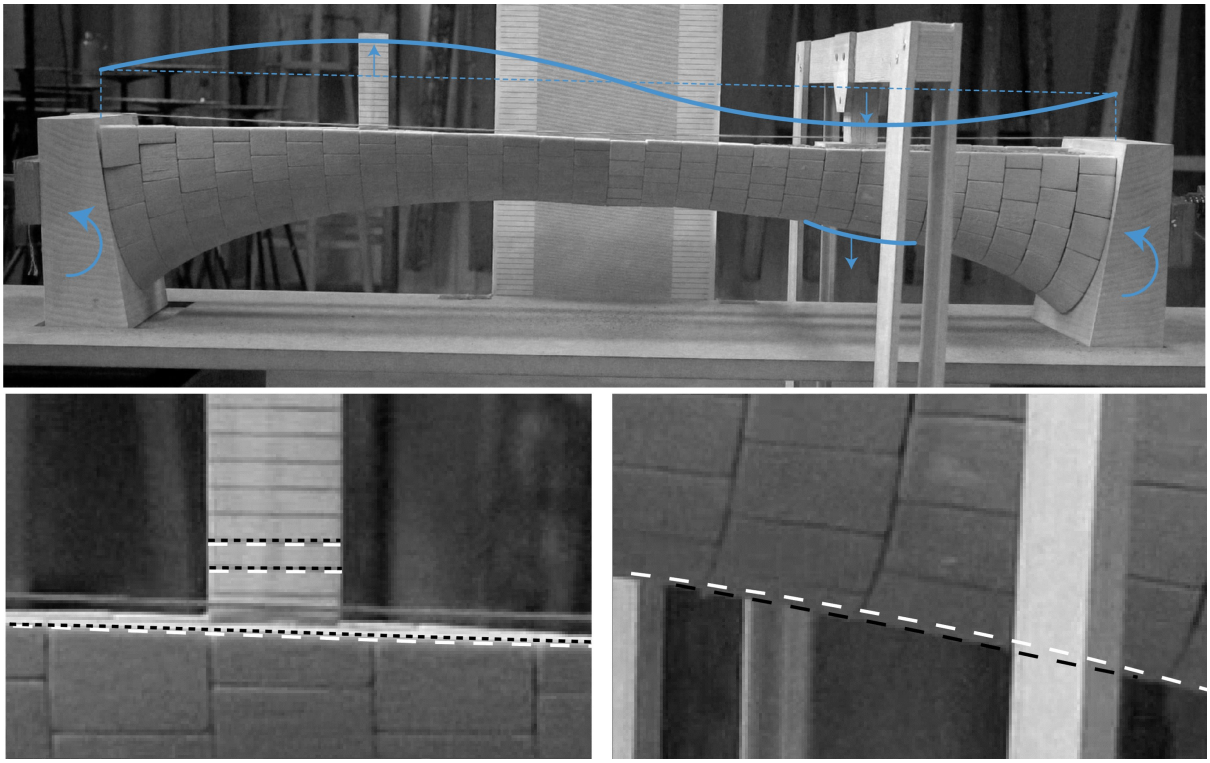

Figure 8: Top, exaggerated deformation pattern in blue after the loading of 19 kg. Bottom left, the upward displacement on the left side around the 1/4 point. The white dashed line shows the initial position and the black dashed line after 19 kg loading. Bottom right shows the local permanent deformation under the load, which decreased the initial curvature (white dashed) to be flat (black dashed).

We have used a 'hard' contact formulation with default enforcement method for the normal behaviour. For the tangential behaviour, we want to ensure that there is no sliding and collapse due to plastic hinges according to Heyman's postulates. Abaqus employs the basic Coulomb friction model $\tau_{crit} = \mu p$, where μ is the friction coefficient and p the contact pressure. To ensure no sliding failure we have used a penalty method with a high friction coefficient of 5 and an infinite elastic slip stiffness as Stagnitta [18].

To run a quasi-static simulation within an explicit framework, damping was added at the contact interfaces, with a coefficient of 0.4. The interaction is modelled with a general contact algorithm.

Loading was performed in two different steps. First, the self-weight of the masonry and fill were applied. Second, the point load was applied and progressively increased to failure.

The self-weight of the voussoirs is defined as a gravity load with magnitude based on volume and density of the material. The load of the fill is modelled as hydrostatic pressure as in (1) and (2), where $\rho = 1600$ kg/m^3 and z is the vertical distance from the top of the bridge. The point load is assumed to spread as a cone with a 45° angle through the fill onto the shell with decreasing magnitude towards the cone surface.

The simulation result is seen in Figure 10. In the top image, just before the collapse, there is a visible bulge under the load and a small lift on the model's underside on the left side. In the bottom image, the load has penetrated the bulge on the right side. This corresponds well to the behaviour in the physical model test, but the collapse load of 14 kN = 1400 kg force which is a factor of 50 times larger. If we assume that this discrepancy is not due to a gross error in the computer model input data, then the most likely cause is the fact that the computer model assumes rigid horizontal supports and does not include geometric imperfections. It is well known in shell theory that geometrical imperfections can have a major impact on collapse load, particularly where buckling is involved.

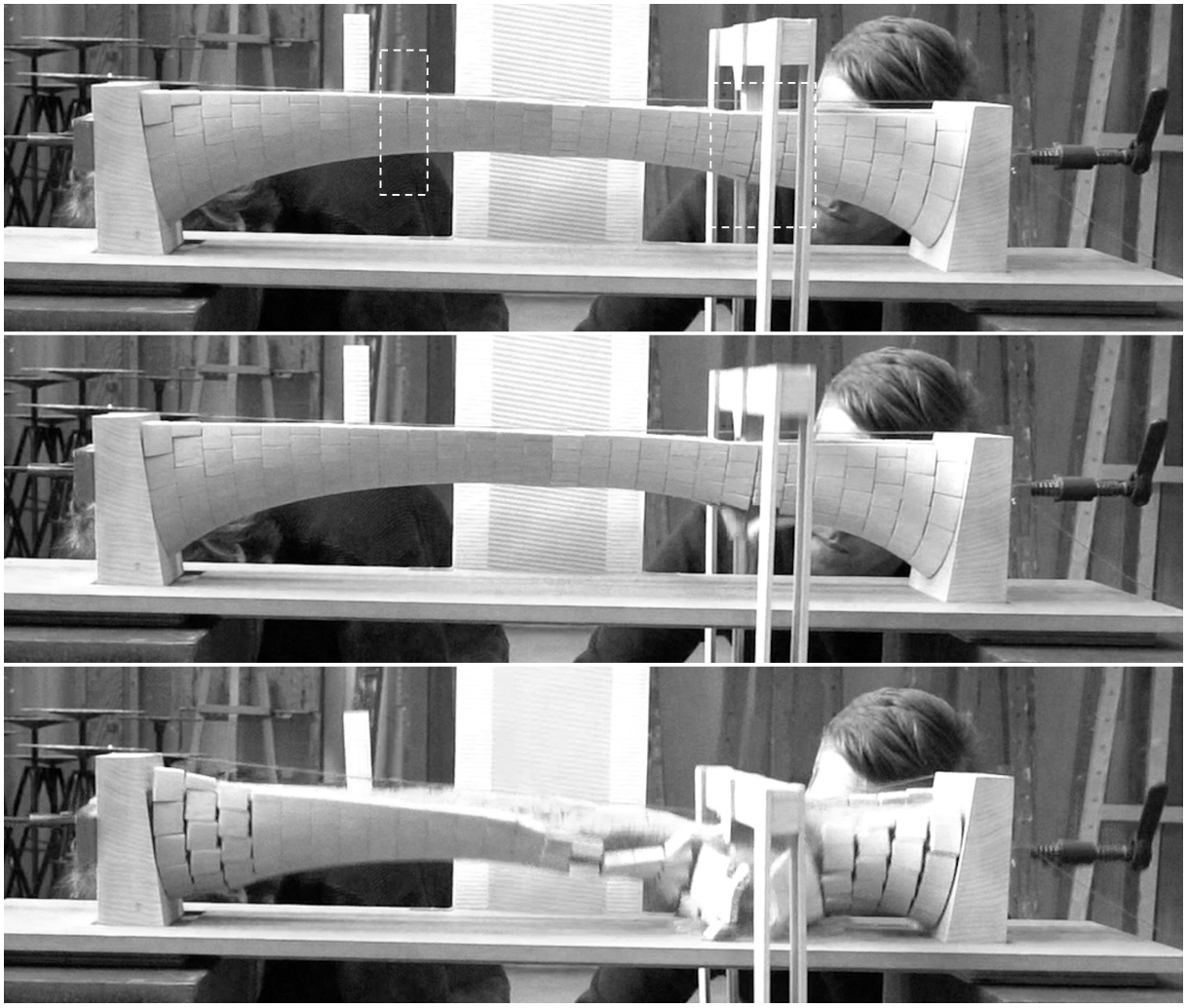

Figure 9: Top, just before the collapsing at 28.9 kg, sand comes out of the bulging crack under the load (white dashed). On the left side, there is a visible crack (white dashed) that opens at the top. Middle, the crack under the load opens up and the rig punches through before the sudden collapse, bottom figure.

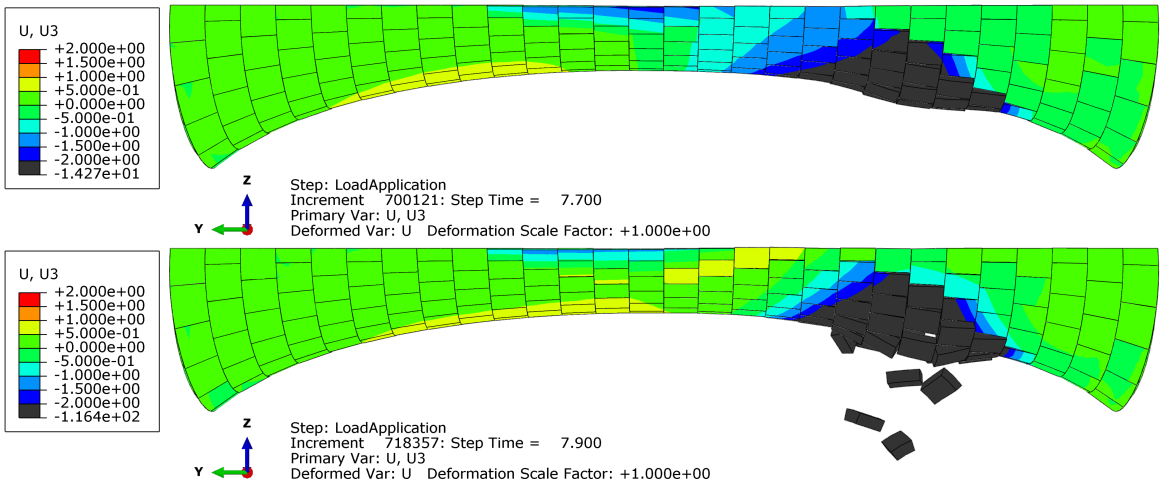

Figure 10: Deformation plots showing the vertical displacements. Top, just before the collapse. In the bottom image, the collapse has been initiated.

5. Conclusions

The physical model behaved well and predicts that the bridge could be used at full scale. Taken as a whole, the bridge is a 3-dimensional thin shell but, in a 2-dimensional projection, acts as a thick arch and therefore the simple failure modes shown in Figure 4 are not kinematically possible. This explains why we have the localised bulging failure shown in Figure 9. This bulging failure is possibly influenced by the horizontal movement of the supports.

The DEM model of the bridge gave qualitatively good results regarding failure mechanisms, but the magnitude of the collapse load obtained was 50 times larger than the load test. We will endeavour to investigate the cause of this discrepancy, but it is believed that it could be caused by the flexibility of the supports and imperfections in the physical model, which were ignored in the computer model, as well as the difficulty in modelling the fill and point load.

References

[1] Z. Orbán, "Assessment, reliability and maintenance of masonry arch railway bridges in Europe," *Proceedings of 4th International Conference on Arch Bridges, Barcelona*, no. 152–161, pp. 1–10, 2004.

[2] L. D. McKibbins, C. Melbourne, N. Sawar, and C. S. Gaillard, "Masonry arch bridges: condition appraisal and remedial treatment," Tech. Rep., 2006.

[3] E. Adiels and C. J. K. Williams, "The construction of new masonry bridges inspired by Paul Séjourné," in *IASS Annual Symposium and Spatial Structures Conference: Inspiring the Next Generation*, Guildford, Surrey, 2021.

[4] J. Heyman, *The masonry arch*. Ellis Horwood Ltd., 1982.

[5] A. Green and W. Zerna, *Theoretical elasticity*, 2nd. Oxford University Press, 1968.

[6] A. S. Day, "An introduction to dynamic relaxation," *The Engineer*, no. 219, pp. 218–221, 1965.

[7] H. J. Schek, "The force density method for form finding and computation of general networks," *Computer Methods in Applied Mechanics and Engineering*, vol. 3, no. 1, pp. 115–134, 1974, ISSN: 00457825. DOI: 10.1016/0045-7825(74)90045-0.

[8] D. J. Struik, *Lectures on classical differential geometry*, 2nd. Dover, 1988, ISBN: 9780486656090.

[9] W. Rankine, *A manual of applied mechanics*, 14th ed. C. Griffin and Co., Limited, 1895. [Online]. Available: https://archive.org/details/cu31924031285384.

[10] J. Heyman, *The Stone Skeleton: Structural Engineering of Masonry Architecture*. Cambridge University Press, 1995.

[11] V. Sarhosis, K. Bagi, J. V. Lemos, and G. Milani, *Computational modeling of masonry structures using the discrete element method*. Hershey PA, USA: Engineering Science Reference (an imprint of IGI Global), 2016, vol. i. DOI: 10.4018/978-1-5225-0231-9.

[12] S. Huerta, *Block models of the masonry arch and vault*. 2020, pp. 31–77, ISBN: 9783433609613. DOI: 10.1002/9783433609613.ch2.

[13] A. Frézier, *La théorie et la pratique de la coupe des pierres et des bois pour la construction des voûtes et autres parties des bâtiments civils & militaires, ou Traité de stéréotomie, à l'usage de l'architecture. Tome 3*. 1739. [Online]. Available: https://gallica.bnf.fr/ark:/12148/bpt6k85688q.

[14] J. Heyman, *Structural analysis: A historical approach*. Cambridge University Press, 1998.

[15] J. Heyman, *Coulomb's memoir on statics: An essay in the history of civil engineering*. Cambridge University Press, 1972.

[16] A. Brencich and R. Morbiducci, "Masonry arches: Historical rules and modern mechanics," *International Journal of Architectural Heritage*, vol. 1, pp. 165–189, 2 May 2007, ISSN: 15583066. DOI: 10.1080/15583050701312926.

[17] E. Adiels, *Hydrostatic masonry bridge load test 1 - Catenary cross section*, 2024. [Online]. Available: https://vimeo.com/921112897.

[18] E. Stagnitta, "Modeling of masonry arch using the discrete element method," Master thesis, Universidad Politécnica de Madrid, 2019.